Tropical Meteorology: Intertropical Convergence Zone

Xianan Jiang[a,b] **and Baijun Tian**[b], [a] Joint Institute for Regional Earth System Science and Engineering, University of California, Los Angeles, Los Angeles, CA, United States; and [b] Jet Propulsion Laboratory, California Institute of Technology, Pasadena, CA, United States

This is an update of D.E. Waliser, X. Jiang, Tropical Meteorology and Climate | Intertropical Convergence Zone, Editor(s): Gerald R. North, John Pyle, Fuqing Zhang, Encyclopedia of Atmospheric Sciences (Second Edition), Academic Press, 2015, Pages 121–131, ISBN 9780123822253, https://doi.org/10.1016/B978-0-12-382225-3.00417-5.

Introduction 1
Mean Structure 2
Seasonal Variations 5
Interannual Fluctuations 7
Subseasonal Variations 8
Linkage Between the ITCZ and Global Climate 10
Representation of the ITCZ in Climate Models 10
Summary 13
References 13
Further Reading 13

Key Points

- Formation of the intertropical convergence zone (ITCZ) is due to meridional gradients in incoming solar radiation, air-sea interaction, and the geometry of continents.
- The ITCZ plays a crucial role in shaping Earth's water and energy cycles.
- Convective activity over the ITCZ exhibits pronounced variability on various time scales.
- The present-day climate models exhibit great challenges in realistically representing the ITCZ and its variability.

Synopsis

The Intertropical Convergence Zone (ITCZ), where surface trade winds converge to form a zone of heavy precipitation, plays a crucial role in the global energy and water cycles. This article summarizes the mean structure of the ITCZ, its induced large-scale circulation and cloud-radiative effects, and the atmosphere-ocean interactive processes underlying the formation of the ITCZ. Variability of the ITCZ on the subseasonal, annual, and interannual time scales will also be presented in the context of its widespread influences on global climate and weather phenomena. Great challenges of present-day climate models in representing the ITCZ and its variability are also discussed.

Introduction

One of the features that is most readily identified with the tropical atmosphere is the Intertropical Convergence Zone (ITCZ). The ITCZ lies in the equatorial trough, a permanent low-pressure zone that marks the meteorological equator where surface trade winds converge to form a region of increased deep convection, cloudiness, and precipitation. The vigorous latent heat released in the convective cloud systems of the ITCZ is critical in driving atmospheric circulation in both tropics and extra-tropics, and plays a crucial role in the global energy and water cycles through coupling with ocean and land. The variability of the ITCZ on various time scales not only exerts tremendous impacts on the occurrence of climate and weather extremes locally and remotely but can also influence the progress of global climate change. Despite the crucial role of the ITCZ in the Earth's climate system, it remains a great challenge for our latest generation climate models in faithfully simulating the ITCZ, noted as a so-called "double-ITCZ" bias.

Mean Structure

Fig. 1 shows the long-term mean rainfall pattern, in which the ITCZ is readily identified as an elongated zonally-oriented (i.e., west to east) band of high rainfall roughly aligned with the equator. The vigorous latent heat release induced by deep convection over the ITCZ generates convergent surface winds onto the ITCZ, which develop into the northeasterly and southeasterly trade winds over the northern and southern hemispheres, respectively, due to the Coriolis effect. The ITCZ rainfall distribution exhibits a fair amount of longitudinal variability. In the eastern Pacific and Atlantic, it is made up of very narrow, intense regions of rainfall to the north of the equator. Over the tropical South American and African continents, the mean rainfall distribution has a considerably larger latitudinal extent and tends to lie directly over the equator. Over the eastern Indian and western Pacific, the rainfall distribution is both broad in latitude and intense in magnitude. Two of the more notable zonal asymmetries in the ITCZ are the rather weak rainfall over the western Indian Ocean and the southeast extension of the ITCZ over the central Pacific Ocean. The latter, referred to as the South Pacific Convergence Zone (SPCZ), leads to an area of intense rainfall on either side of the equator with a relatively dry region in between. Such a structure is often referred to as a "double ITCZ."

While a well-defined ITCZ rain belt is clearly evident in the long-term mean rainfall pattern in Fig. 1, on any given day in the Tropics, there are usually a number of deep convective cloud systems that appear to be somewhat randomly distributed across the climatological ITCZ zone. Fig. 2 shows a satellite cloud image constructed from the National Oceanic and Atmospheric Administration's (NOAA) GEOS-11 geostationary satellite on August 13, 2009. Bright white areas denote high and deep clouds, and indicate clouds whose tops are at or near the level of the tropopause, e.g., deep convective clouds. Grayish white areas denote mid-level and circus clouds, in this case implies convective clouds during their developing or decaying phases. The convective clouds along the Pacific ITCZ exhibit organization across multiple spatial scales, ranging from large cloud systems with a horizonal scale of several thousand kilometers, to small scale clouds on an order of a few hundred kilometers or less. The size of the various cloud systems shown in Fig. 2 can be influenced by their maturity stage and their abundance in any one area. For example, deep convective "towers" typically have horizontal scales on the order of 1−10 km and when found in isolation usually indicate young or developing convective system. Cirrus clouds can appear to extend over thousands of kilometers and encompass tens or hundreds of convective towers simultaneously. Embedded in these systems, there are remnants of the Tropical Storm Maka and Hurricane Felicia, the active Tropical Depression 9E, and a new tropical storm named Guillermo over the eastern Pacific before it developed into a category-3 hurricane.

While most cloud systems in the tropics arise from simple convective instability, likely in conjunction with synoptic wave-like disturbances inherent to the equatorial region, the organization of some systems can be influenced by low-frequency phenomena which can increase their spatial extent. For example, the larger systems in the Indian and western Pacific Ocean may be influenced by the Madden-Julian Oscillation (MJO; Madden and Julian, 1971; Jiang et al., 2020) or simply be larger due to the difference in climatological conditions (e.g., sea surface temperature, SST) between the eastern and western hemispheres which are discussed below.

The time-mean spatial structure of the ITCZ shown in Fig. 1 can be better understood by examining the time-mean SST, as shown in Fig. 3. Because on average the equatorial region receives the most solar irradiance, this region also tends to have the highest SSTs. While this tendency for very warm SST (i.e., greater than 27 °C) is mostly uniform with longitude, there are some deviations. These deviations are produced by a number of factors, including ocean basin geometry, ocean circulation properties—equatorial dynamics in particular, as well as the coupled interaction with the atmosphere, including the ITCZ itself. For example, a strong zonal gradient in the SST pattern is observed across the equatorial Pacific and Atlantic, with large patches of warm water piling up over the western part of these ocean basins, collocated with strongest rainfall over the ITCZ, particularly over the western Pacific. In contrast, the SST patterns over the east Pacific and Atlantic are characterized by a "cold-tongue" structure with presence of cool SST near the equator and over the southeastern parts of these regions, in association with largely suppressed local rainfall. The strong zonal asymmetry in SST patterns across the tropical Pacific and Atlantic is mainly caused by the prevailing easterly trade winds, which generates an east-west tilting in the ocean thermocline depth (Fig. 3). The shallow thermocline over the eastern part of these ocean basins

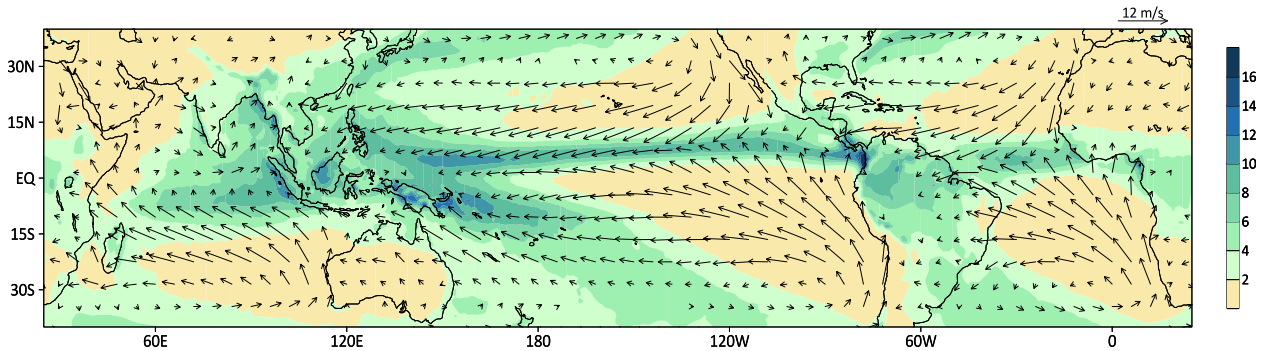

Fig. 1 Long-term mean (2000 to 2022) surface rainfall rate (unit: mm day^{-1}) based on satellite observations from the National Aeronautics and Space Administration's (NASA) Global Precipitation Measurement (GPM) mission, the Integrated Multi-satellitE Retrievals for GPM (IMERG; version 7), and surface winds (unit: m s^{-1}, see the vector scale on upper-right) based on the fifth generation ECMWF atmospheric reanalysis dataset (ERA5).

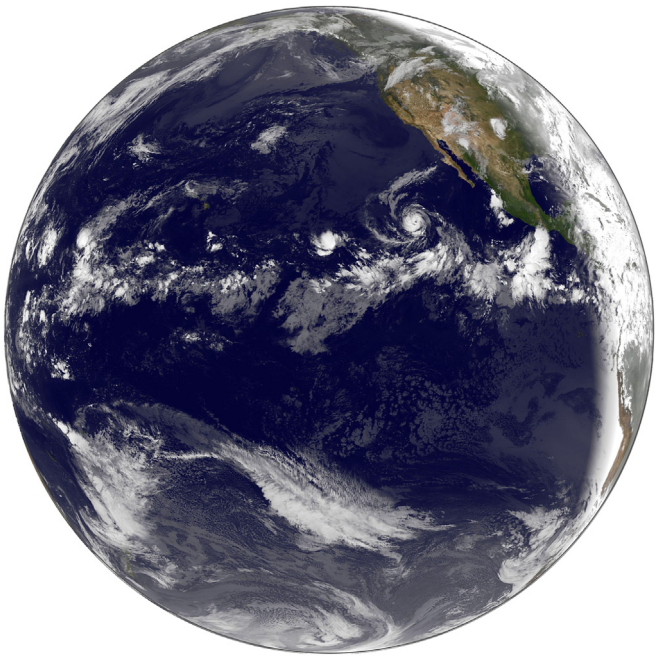

Fig. 2 A snapshot of multiscale tropical convective clouds along the ITCZ over the Pacific Ocean observed by NOAA GOES-11 on August 13, 2009. *Image courtesy* of OAA/NASA GOES Project.

promotes upwelling of cold water, leading to relatively cool SST. On the other hand, the northward displacement of the ITCZ about the equator over the eastern Pacific and Atlantic is in accord with the northward shifted warm SST brands. This north-south asymmetry in ITCZ rainfall and SST patterns over these regions is initially induced by the continental geometry over the equatorial South America and Africa, and enhanced by a positive feedback due to interactions of surface wind, evaporation and SST, along with a positive feedback between SST and low-level stratus clouds that shield incoming solar radiation over the cold water region of the southeast tropical Pacific and Atlantic (Xie, 2004).

Why tropical convection favors the warm ocean surface such as over the ITCZ region? The relatively warm water over the equatorial region heats the air in the lower atmosphere making it less dense and more buoyant relative to the air aloft. This buoyancy forcing leads to rising motion over the equatorial region. As the moist near-surface air rises, it cools adiabatically and begins to undergo condensation which releases the latent heat due to phase change from water vapor to cloud water and produces rainfall at the surface. This latent heating enhances the buoyancy and associated upward motion of the air even further, which in turn enhances the adiabatic cooling, water vapor condensation and surface rainfall. This process continues until nearly all the water vapor condenses out of the parcel and/or the parcel is no longer buoyant with respect to its environment. Over the warmest tropical ocean, this often happens when the convective parcel reaches the inversion associated with the tropopause, whereupon the air begins to move away from the equator. This divergent upper-level air undergoes cooling through radiative heat loss, causing it to lose buoyancy, and sinks in the subtropical regions.

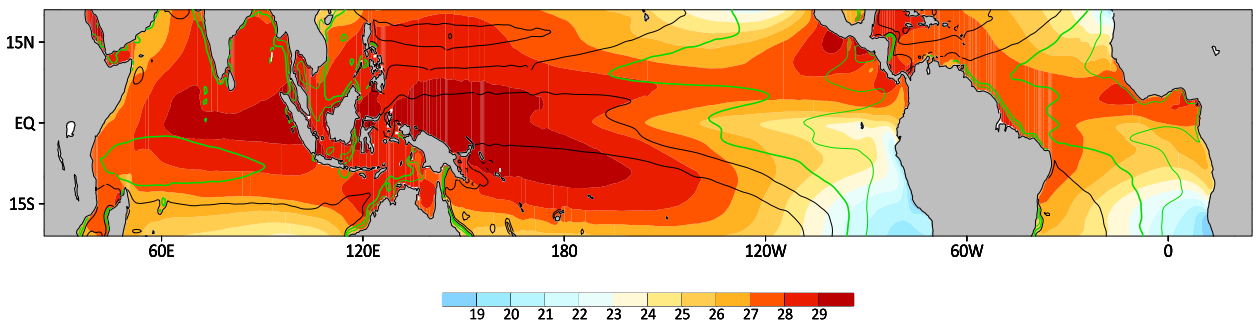

Fig. 3 Long-term mean sea surface temperature (SST; shaded with unit of ^{o}C) based on NOAA Optimum Interpolation Sea Surface Temperature (OISST) analysis and 20 °C isothermal depth (contours at 50 m intervals with values $\leq$ 100 m in green, and the thick green line for 100 m depth), based on the European Centre for Medium-Range Weather Forecasts (ECMWF) Ocean Reanalysis System 5 (ORAS5) global ocean reanalysis monthly data.

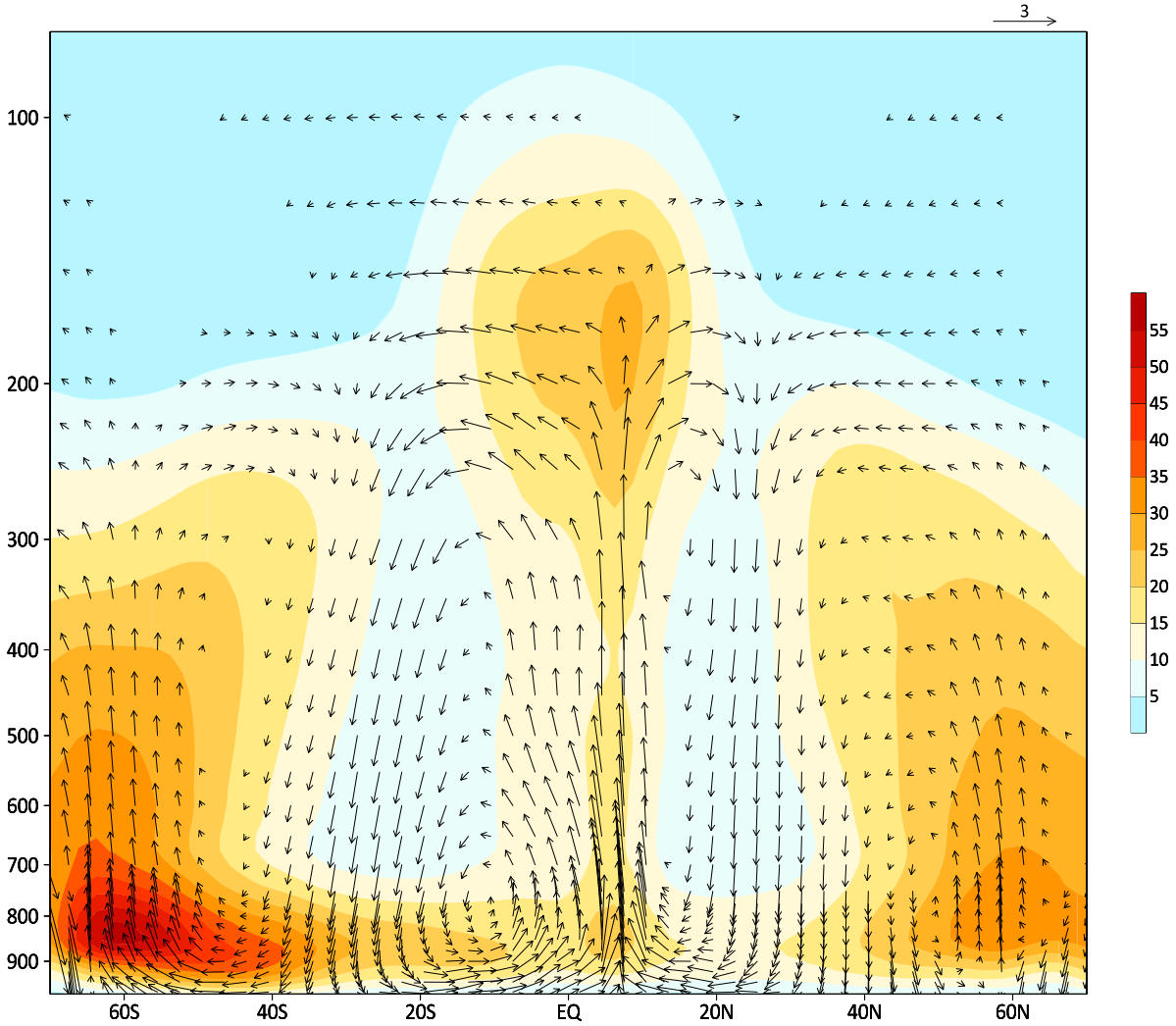

Fig. 4 Vertical-latitudinal cross-section of long-term mean zonally-averaged cloud fraction (shading) from climatology for 2006–2018, based on the combined NASA CloudSat and Cloud-Aerosol Lidar and Infrared Pathfinder Satellite Observations (CALIPSO) satellites, and climatological meridional–vertical wind vectors for 2001–2020 based on ERA5 reanalysis dataset (see the vector scale on the upper-right side, with units of m s^{-1} for v-wind and 100 Pa s^{-1} for pressure-level vertical velocity ω, and with sign reversed for ω).

The collective effects of deep convection along the ITCZ as described above is illustrated by CloudSat/Cloud-Aerosol Lidar and Infrared Pathfinder Satellite Observations (CALIPSO) satellites and other combined observations in Fig. 4, which shows the long-term zonal mean vertical cloud and wind structure along the latitudes. A narrow band of strong upward motion is readily discerned over the ITCZ region near 6°N, extending from the surface to the upper-troposphere near 150 hPa (~14 km), in association with deep clouds stretching almost the entire troposphere with widespread cirrus clouds at the top. The strong rising motion over the ITCZ is associated with the low-level convergent meridional winds onto the ITCZ, with divergent upper-level winds towards the poles and slowly descends, leading to large areas of high pressure in the subtropics in both hemispheres. The resulting circulation with rising motion over the ITCZ region and descending motion over the subtropics on both sides of the ITCZ is known as the "Hadley Circulation."

Fig. 5 depicts the long-term mean distribution of high and low cloud fractions derived from the Moderate Resolution Imaging Spectroradiometer (MODIS) instrument. The pattern of high cloud fractions (Fig. 5A) largely follows the mean rainfall pattern in Fig. 1, suggesting the development of deep convective clouds within the ITCZ as discussed above. Meanwhile, low clouds prevail over subtropical regions over the eastern Pacific and Atlantic, as well as in the southern Indian Ocean (Fig. 5B). Maximum low cloud fractions are evident over the eastern portions of these ocean basins, largely due to coastal oceanic upwelling induced by the trade winds and downward motion in the subtropical high region over the descending branches of the Hadley circulation (Fig. 4). Prevalence of low clouds over the eastern subtropical Pacific Ocean can also be seen by the dark grayish areas in the NOAA GEOS-11 satellite image in Fig. 2.

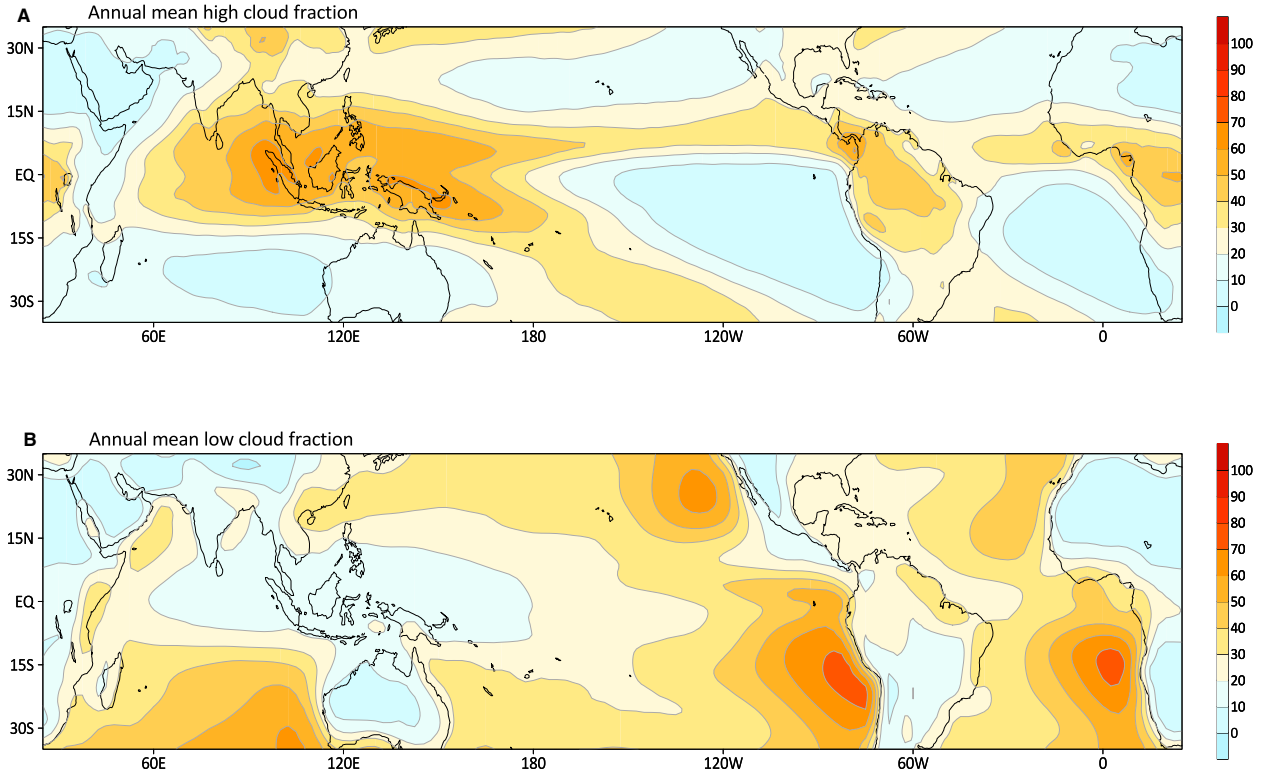

Fig. 5 Long-term mean (2002–2022) satellite-derived cloud fraction maps by the NASA's Moderate Resolution Imaging Spectroradiometer (MODIS) instrument: (A) high clouds; (B) low clouds.

The cloud patterns associated with deep convection over the ITCZ region and its induced Hadley circulation significantly influence Earth's energy balance by reflecting shortwave solar radiation back to space to cool the Earth, absorbing longwave radiation emitted by Earth's surface and atmosphere, and emitting longwave radiation by themselves. Fig. 6A shows the long-term mean outgoing longwave radiation (OLR) leaving the top of the atmosphere. The regions of large radiative heat loss lie over deserts and equatorial dry zones where a warm surface is overlaid by a relatively dry and cloudless atmosphere, allowing more radiation emitted by the Earth's surface to pass through the atmosphere. The regions of low OLR mainly lie over the ITCZ region, with lowest values over the Maritime Continent due to the prevalence of deep convective clouds with high and cold tops. Here the radiation emitted by the Earth's surface and atmosphere is absorbed by clouds and reemitted by these clouds at a much lower temperature. Meanwhile, the maxima of reflected shortwave radiation are found over the tropical ITCZ region and subtropical regions where thick clouds are plentiful or over bright surfaces such as the Sahara Desert (Fig. 6B), i.e., with the largest planetary albedos for the incoming solar radiation. The smallest reflected shortwave radiation is evident over tropical and subtropical oceans with sparsely-distributed clouds, where annual-mean local albedos can range as low as 0.10.

Seasonal Variations

Over the course of the annual cycle, seasonal changes occurring in the ITCZ modify the mean structure depicted in Fig. 1. In general, the entire zonally-oriented convection band marches north in the Northern Hemisphere summer and south in the boreal winter (Fig. 7), with the annual cycle of the global ITCZ rainfall exhibiting a modest resemblance to a sinusoidal pattern (Fig. 8F). The differences in the amplitudes and phases of the ITCZ excursions at different longitudes are dictated in part by the different characteristics of the surface (i.e., land or ocean) and the local atmospheric circulation pattern. The ITCZ over land (e.g., Africa and S. America) largely follows the annual march of the Sun, while the migration of the ITCZ over extended ocean regions lags slightly behind the Sun by a month or two (Fig. 8). This time lag is most apparent in the eastern Pacific and the Atlantic Oceans, where the ITCZ is furthest south in the Northern Hemisphere spring and furthest north in the Northern Hemisphere fall. The origin of this time lag is primarily due to the large thermal inertia of the ocean mixed-layer compared to the land surface but also involves complex dynamical interactions that develop between the ocean and atmosphere.

While most of the seasonal changes in the ITCZ are associated with latitudinal migration, there are other significant structural changes. One of the most significant of these is over S. America where large spatial differences exist between the "ITCZs" of the boreal summer and winter (Fig. 7). During the boreal winter, the rainy season encompasses nearly the entire tropical area of the

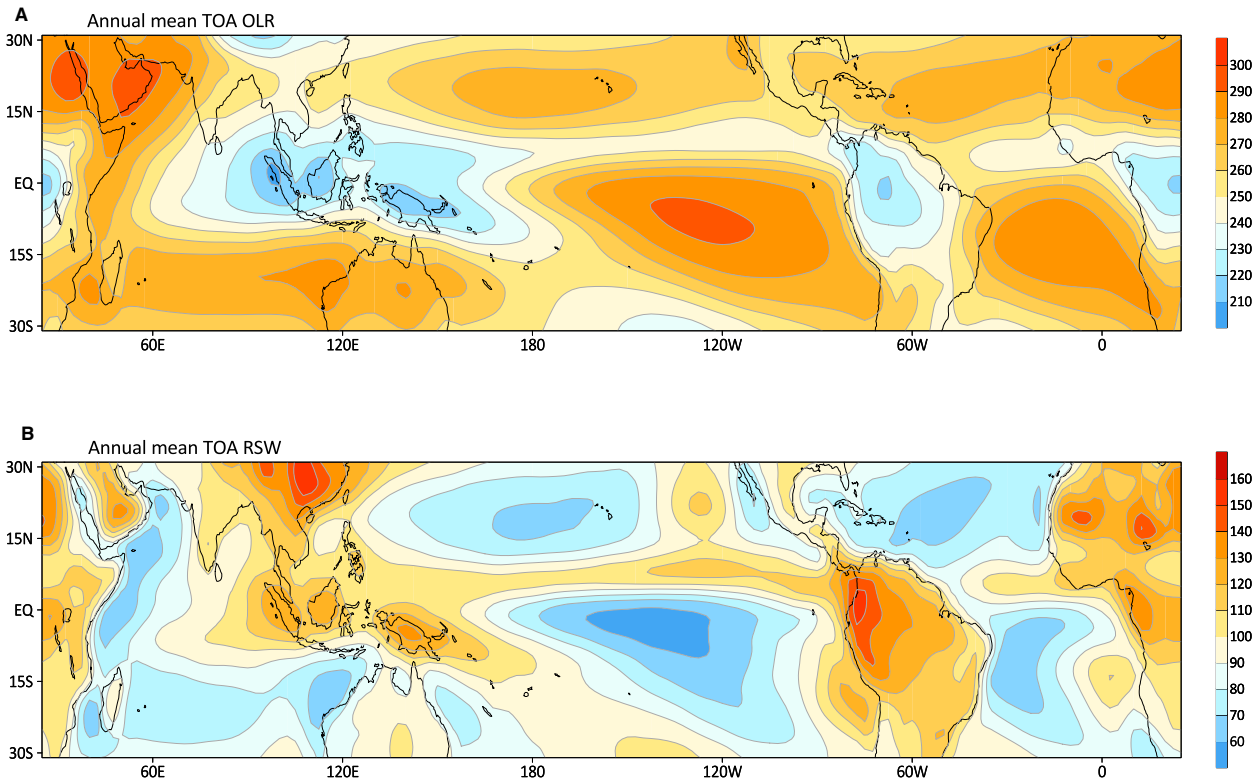

Fig. 6 Long-term mean (2001–2023) satellite-derived radiative flux patterns at the top of the atmosphere (TOA) by the NASA's Clouds and the Earth's Radiant Energy System (CERES) instrument: (A) outgoing longwave radiation (OLR); (B) upwelling or reflective shortwave radiation (RSW).

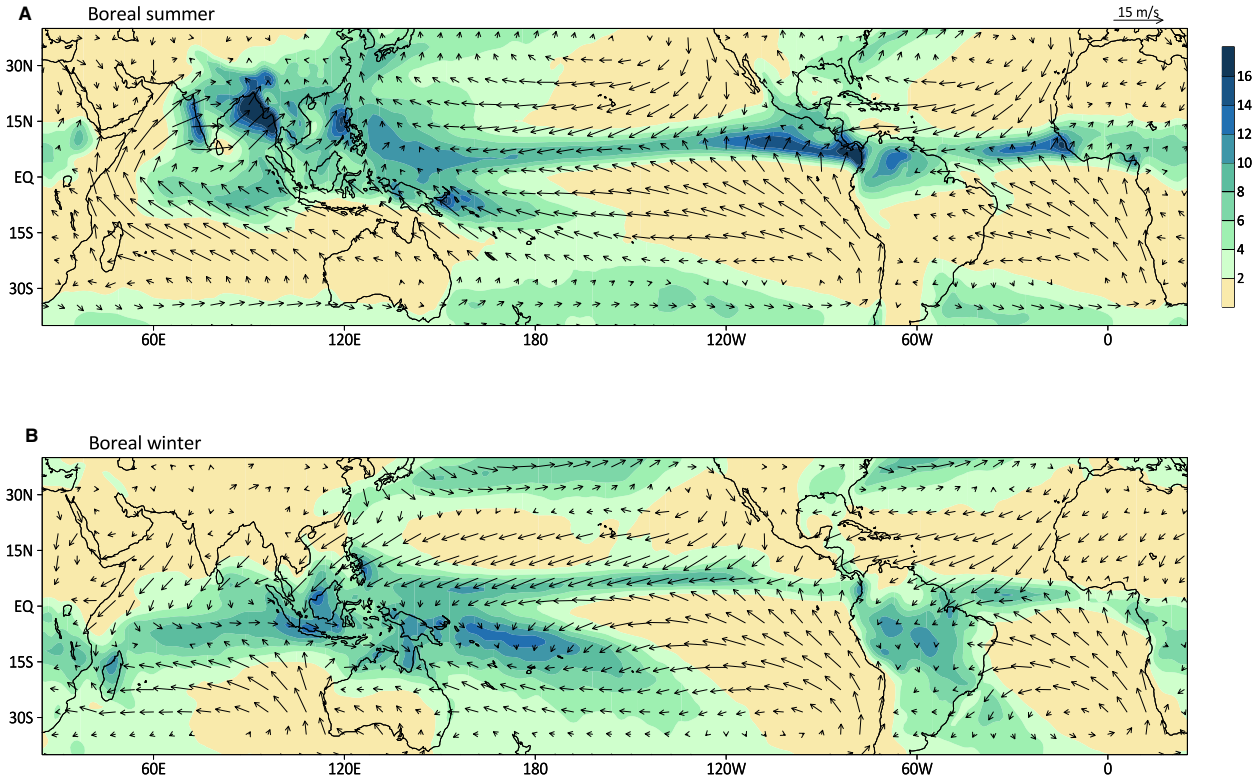

Fig. 7 Same as in Fig. 1 but for long-term rainfall climatology during the boreal summer (June-August; Panel (A) and winter (December-February; Panel (B).

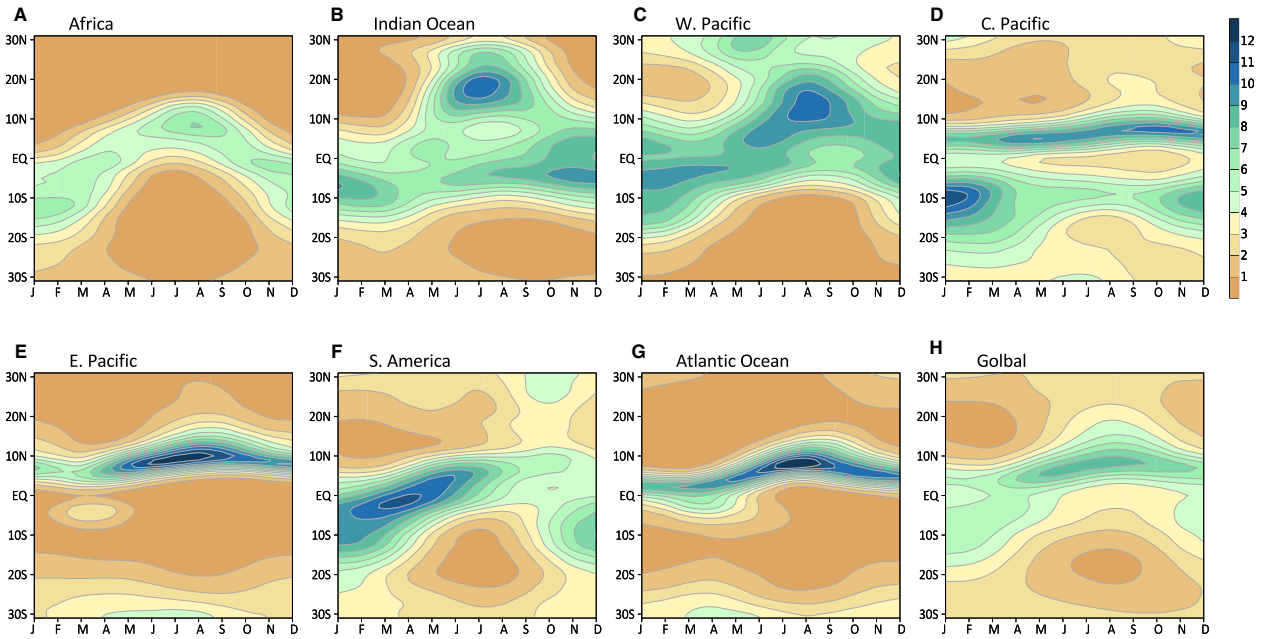

Fig. 8 Time-latitude diagrams of the annual cycle of the ITCZ, in terms of rainfall (unit: mm day^{-1}), zonally averaged over eight different longitude sectors: (A) Africa, 10-40°E; (B) Indian Ocean, 60-100°E; (C) Western Pacific, 110-150°E; (D) Central Pacific, 160°E-160°W; (E) Eastern Pacific, 100-140°W; (F) South America, 45-75°W; (G) Atlantic, 10-40°W; (H) Global, 0-360°E. Mean annual cycles were computed from the period 2000 to 2022 based on the NASA GPM-IMERG satellite observations.

South American continent. This produces a latitudinally and longitudinally broad ITCZ. In the boreal summer, the ITCZ overlies the northern end of the continent and has a structure more consistent with its oceanic counterparts to the east and west. The annual cycle of the ITCZ over S. America displays the least amount of symmetry with respect to north-south migration and ITCZ intensity.

Another dramatic seasonal change associated with the ITCZ occurs in the Indian Ocean region during the Asian summer monsoon. As the monsoon circulation develops and intensifies, the convection zone splits, with a very intense area of rainfall occurring over the Indian subcontinent and a weaker rainfall maximum remaining in the equatorial region (Figs. 7A and 8B). A similar intensification of rainfall occurs over northern Australia during the Southern Hemisphere summer. During this same period, the convergence zones over Africa and the Indian Ocean become more continuous due to the reduced coastal ocean upwelling off the east African coast (Fig. 7B).

The ITCZ over the eastern Pacific remains primarily in the northern hemisphere throughout the year, with the most intense ITCZ in the Northern Hemisphere fall when the surface water associated with the equatorial countercurrents is warmest and the low-level trade wind convergence is strongest. In addition, some weak rainfall occurs south of the equator in the Northern Hemisphere spring. During this time of year, warm water (~27 °C or greater) occurs on both sides of the equator in this region and the ITCZ, in its southern most position, is split by a zone of equatorial ocean upwelling (i.e., cool equatorial SSTs), leaving two zones of convection straddling the equator (Fig. 8E). This "double ITCZs" results from a relaxation of the southeast trade winds, which greatly diminishes the equatorial and nearby coastal ocean upwelling leaving seasonably warm surface temperatures south of the equator. A very similar seasonal migration of the ITCZ is also found over the Atlantic Ocean (Fig. 8G). In a related manner, while the ITCZ in the central Pacific is composed of northern and southern convergence zones straddling the equator, the two branches of convergence oscillate in strength during the year with the southern and northern branches intensifying during their respective summer season (Fig. 8D).

Interannual Fluctuations

Apart from the regular seasonal variations, the ITCZ undergoes pronounced interannual fluctuations in its position and intensity, for example, under the influences by the climate phenomena known as the El Niño-Southern Oscillation (ENSO). In warm phases of ENSO (i.e., El Niño), SST in the central and eastern equatorial Pacific Ocean can become anomalously warmer by about 1-3 °C while in cold phases (i.e., La Niña) this region becomes anomalously colder by a similar magnitude. At the peak phase of a typical El Niño event (December), due to the building up of a large area of warm water over the normally equatorial cold tongue region of the central and eastern Pacific, the ITCZ and the belt of heavy rainfall over the western Pacific shift to the east of the International Date Line, normally an equatorial dry zone, bringing heavy rainfall to the Pacific islands that lie close to the equator and to the coastal regions of equatorial South America, such as Ecuador and Peru (Fig. 9). In contrast, extreme heat and drought are usually observed over most of Amazonian rainforests, particularly over eastern Amazonia, forming a zonal wet-dry dipole pattern in precipitation over equatorial South America. A significant reduction in rainfall can be also observed over eastern and northern Australia, and

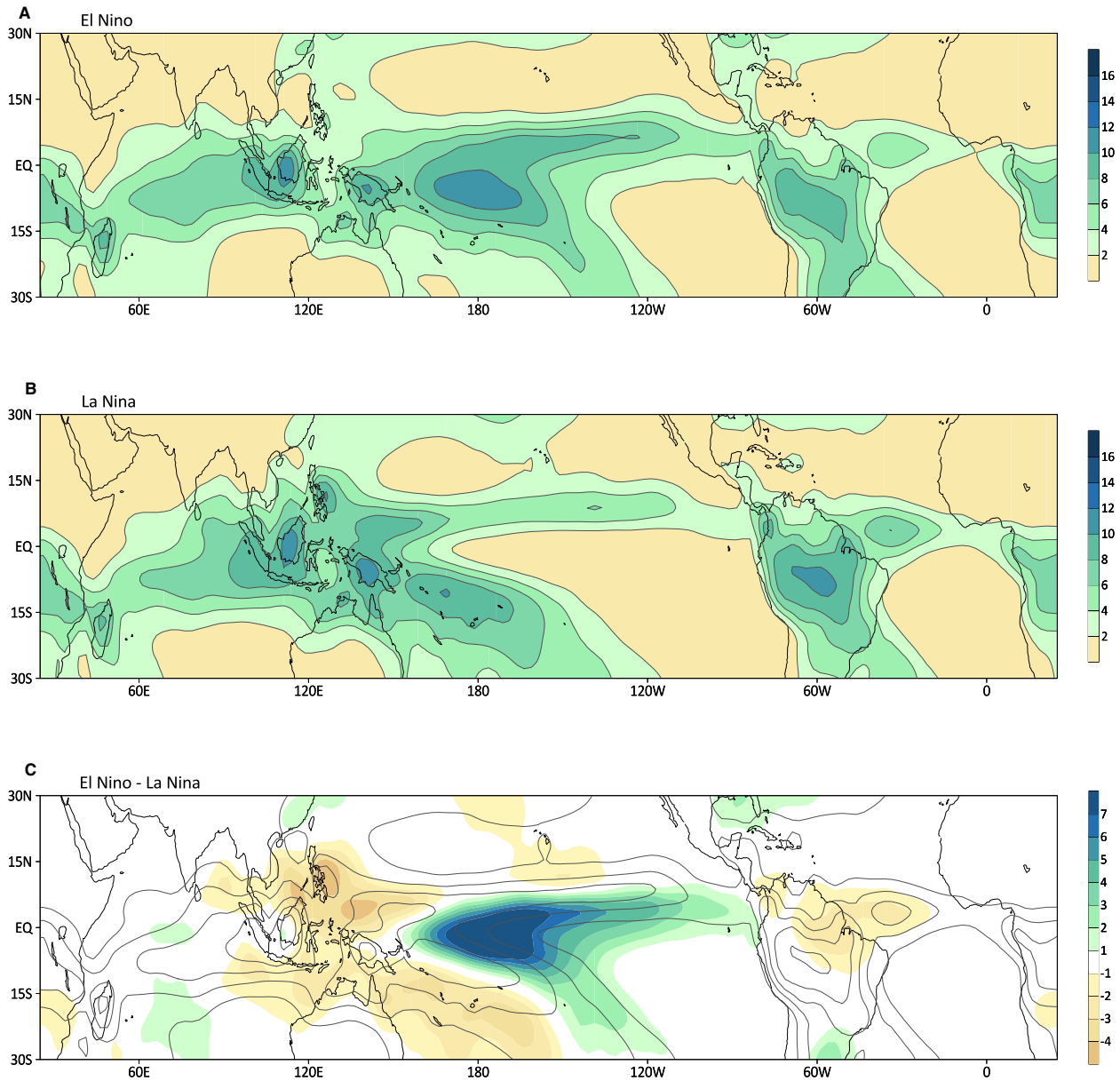

Fig. 9 Composite boreal winter (November-March) mean rainfall patterns for typical (A) El Niño and (B) La Niña conditions, and their difference (El Niño minus La Niña) as denoted by shaded contours in (C) along with 1979–2020 climatological boreal winter mean rainfall pattern in line contours. Typical El Niño (La Niña) conditions are defined by the November-March averaged NOAA Niño3.4 index with the values above 0.8 °C (below −0.8 °C) for El Niño (La Niña) conditions, resulting in a total of 8 El Niño events and 8 La Niña winters during the period of 1979–2020. Rainfall data is based on NOAA's Global Precipitation Climatology Project (GPCP) product, which integrates various satellite datasets over land and ocean and a gauge analysis over land.

over the Maritime Continent islands, raising the risk of widespread wildfires. A southward movement of the ITCZ band over the eastern Pacific is observed during the El Niño winters. Changes in the rainfall pattern over the ITCZ region during a typical La Niña winter are largely opposite to the El Niño, during which a relatively dry equatorial zone is formed near the International Date Line, leaving the elongated ITCZ belt stretching further west towards the western Pacific than normal.

Subseasonal Variations

The ITCZ also exhibits strong variability on subseasonal time scales. Fig. 10 shows how rain pattern over the ITCZ changes with the Madden-Julian Oscillation (MJO), the most prominent subseasonal variability mode in the tropics. Unlike ENSO, which is

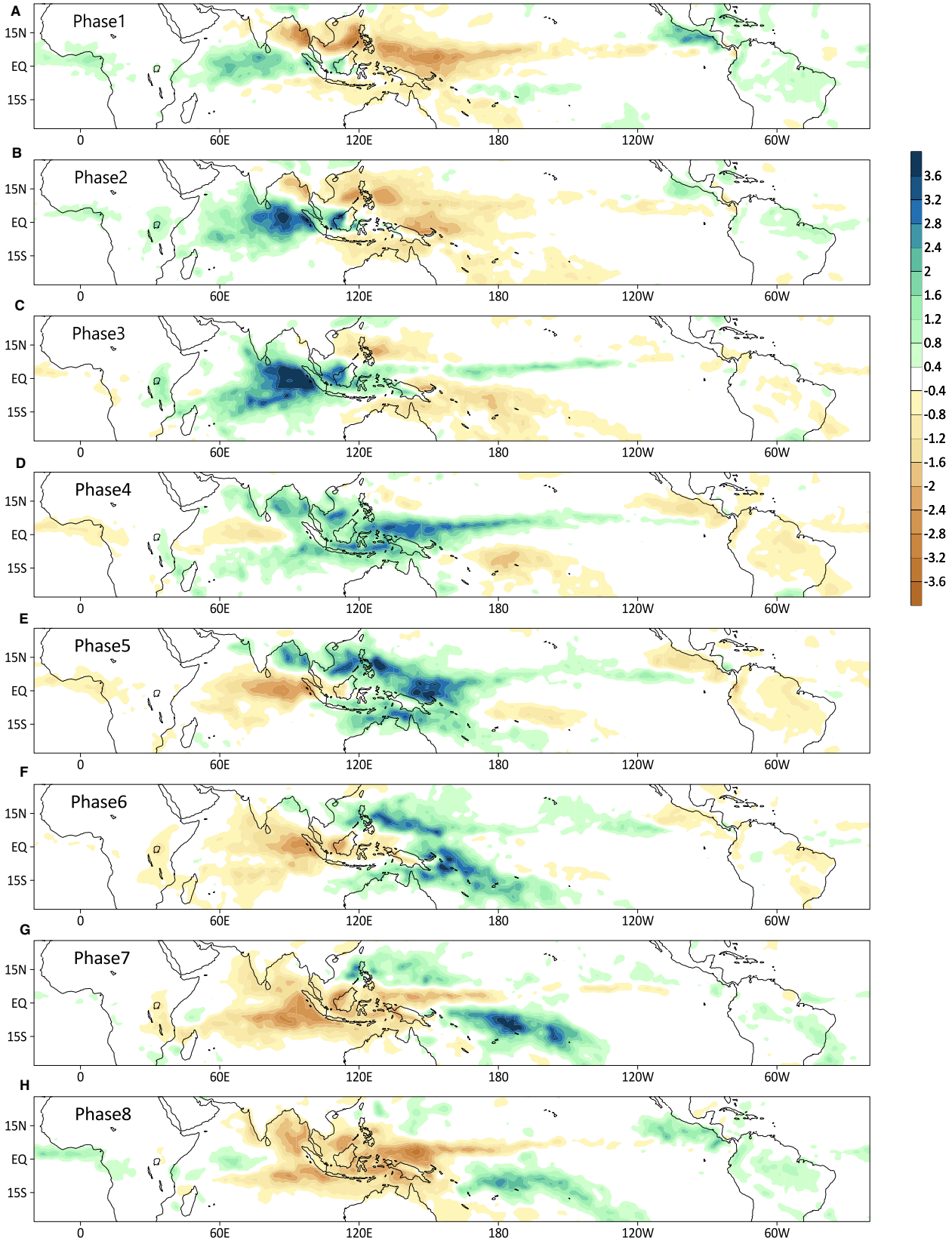

Fig. 10 Composite rainfall anomalies (mm day^{-1}) during the eight phases (panels a-h) of the MJO. For a typical MJO cycle of 30–60 days, each phase takes about 5–7 days. Rainfall anomalies shown here represent departures from the long-term mean rainfall climatology. The daily MJO phase is defined by the RMM MJO index. The daily rainfall data is from NASA GPM IMERG for 2000–2022.

stationary, the MJO is an eastward moving disturbance of clouds, rainfall, winds, and pressure that traverses the global tropics roughly with a period of 30 to 60 days (Madden and Julian, 1971; Jiang et al., 2020). Here a complete cycle of a typical MJO is separated into eight phases based on the real-time multivariant MJO (RMM) indices developed at the Australian Bureau of Meteorology (Wheeler and Hendon, 2004). By the definition, each phase encompasses about 5−7 days during a typical MJO cycle.

The eastward propagation of active MJO convection along the equator is readily seen in **Fig. 10**. After its formation over the western equatorial Indian Ocean at Phase 8, the MJO convection becomes significantly enhanced over the central and eastern Indian Ocean at Phases 1−3, and then moves over the Maritime Content towards the western Pacific during Phases 4−5. Meanwhile, enhanced rainfall is discerned along the Pacific ITCZ belt extending far into the eastern Pacific, indicative of fast-moving equatorial Kelvin waves emitted from the MJO convection over the western Pacific, which bridge the MJO variability across ocean basins. After Phase 5, while enhanced MJO convective signals continue moving eastward crossing the SPCZ region near the central Pacific, the east Pacific, the Amazon area, and the tropical Atlantic Ocean, the Indo-Pacific region is replaced by a break cycle of the MJO with development of suppressed convection over the Indo-Pacific region and a similar eastward movement.

In addition to the eastward propagation of the MJO disturbance, which is most favorable during the boreal winter season, MJO convective variability also exhibits pronounced poleward migration during boreal summer (Yasunari, 1979; Sikka and Gadgil, 1980). As seen in **Fig. 10**, a northwestward-tilted rain band develops at Phase 4, stretching from India to the Maritime Continent and equatorial western Pacific. This slanted band of active convection then propagates northward in association with the eastward phase propagation along the equator. Over the India Ocean sector, the northward propagating MJO convection from the equatorial region to the Indian subcontinent plays a crucial role in modulating the onset as well as the active and break phases of the Indian monsoon (Sikka and Gadgil, 1980; Lawrence and Webster, 2002). Similar northward propagating MJO signals are also found over the eastern Pacific warm pool region during boreal summer associated with the North American monsoon (Jiang and Waliser, 2008), e.g., at Phase 8−2 in **Fig. 10**, although not as pronounced as its counterpart over the Asian monsoon region. The northward propagation of MJO is generally considered to be resulted from interaction between the MJO convection and easterly vertical wind shear associated with the summer monsoon circulation over these regions (Jiang et al., 2004).

During boreal summer, the warm SST and convergence of surface trade winds over the ITCZ region provide a favorable environment for genesis of tropical cyclones. Given the strong modulation of the ITCZ by the MJO, tropical cyclone activity over global oceans is significantly influenced by MJO phases (Nakazawa, 1988; Maloney and Hartmann, 2000; Bessafi and Wheeler, 2006; Jiang et al., 2012). A majority of tropical cyclogenesis over the western North Pacific tends to occur during the MJO Phase 4−6, when the MJO convection is active in this region and its associated large-scale environmental conditions, including enhanced mid-tropospheric moisture and low-level cyclonic flow, are in favor of tropical cyclogenesis (Camargo et al., 2009).

Linkage Between the ITCZ and Global Climate

As discussed in previous sections, the ITCZ exerts significant impacts on weather and climate phenomena in the tropics and subtropics, including the mean precipitation pattern and precipitation extremes such as hurricanes, the Hadley circulation and its induced moisture and energy transport, clouds and associated energy balances, as well as low-frequency tropical variability such as the MJO and ENSO. The ITCZ is also critical in shaping the climate variability and change over the mid-to-high latitudes through planetary Rossby-wave teleconnection patterns. **Fig. 11**A shows anomalous circulation patterns at 500 hPa during a typical El Niño winter, denoted by the geopotential height perturbations as a departure from the long-term mean, which is characterized by a so-called Pacific-North American (PNA) pattern (Wallace and Gutzler, 1981), with a low-pressure system (e.g., an extratropical cyclone) situated over the eastern North Pacific off the west coast of US. Enhanced moisture transport along with elevated atmospheric river activity due to strengthening of the westerly jet stream in the southern part of this Pacific low tends to promote enhanced precipitation over west coast US., including the California region, during an El Niño winter. Opposite situations can occur during an La Niña winter. This PNA-like pattern also leads to widespread variations in surface temperature over the globe, which can even slow or accelerate the global warming rate from the CO_2 induced radiative forcing. For example, the persistent La Niña-like SST pattern over the eastern Pacific and its induced global Rossby wave patterns were considered crucial in leading to the climate warming hiatus during 1998−2014 (Kosaka and Xie, 2013; Xie and Kosaka, 2017).

The ITCZ rainfall variability associated with the MJO can similarly induce widespread influences on the mid-to-high latitudes through emanation of the planetary Rossby waves (Jiang et al., 2020, **Fig. 11**B). For example, studies suggest that the recent rapid warming over Arctic could be partially as a response to more frequent MJO convective activity over the Maritime Continent and western Pacific, through enhanced moisture transport and warm temperature advection into the Arctic by planetary Rossby waves (Lee et al., 2011; Yoo et al., 2012). The MJO can also influence the sudden stratospheric warming events which could further lead to a distorted or completely reversed stratospheric polar vortex and modulate the phase of the Northern Hemisphere Annular Mode (Garfinkel et al., 2012; Kang and Tziperman, 2018).

Representation of the ITCZ in Climate Models

Despite the crucial role of the ITCZ in the global climate system, our latest atmosphere-ocean coupled global climate models, however, cannot well simulate the location and strength of the ITCZ. For example, most models tend to simulate a spurious

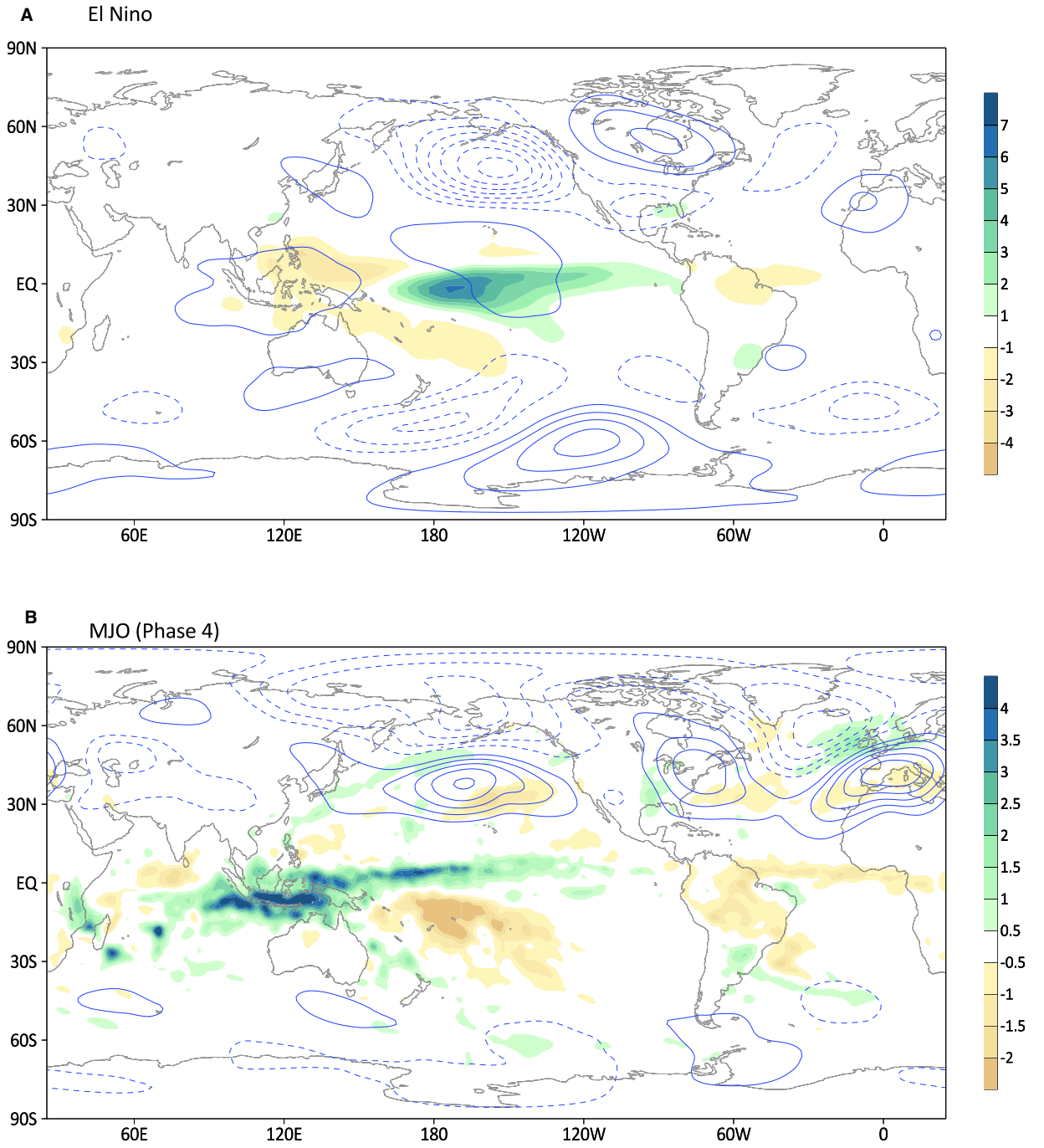

Fig. 11 (A) Composite anomalous mean rainfall (shaded; units: mm day^{-1}) and geopotential height at 500 hPa (contours) during a typical El Niño winter (November-March) based on 8 El Niño winters during 1979–2020 as defined in **Fig. 9**; (B) Similar as in **Fig. 10**, but for composite rainfall (shaded) and geopotential height at 500 hPa (contours) anomalies for the MJO Phase 4 during the boreal winter (November-March) for 2000–2020. Both rainfall and geopotential height anomalies are defined by the departures from their corresponding long-term climatology. Geopotential height anomalies in both panels, based on ECMWF ERA5 reanalysis dataset, have the unit of geopotential meter (gpm), with a contour interval of 100 gpm, solid (dashed) lines for positive (negative) values, and zero lines omitted.

ITCZ over the southeastern Pacific and the southern Atlantic parallel to the equator near 10°S, and thus two ITCZs instead of a single ITCZ to north of the equator in observations. As a result, there is excessive rainfall and high clouds south of the equator, while insufficient rainfall and high clouds near the equator in most of coupled models (**Fig. 12**). This is referred to as the notorious "double-ITCZ" bias in climate models (e.g., Hwang and Frierson, 2013; Li and Xie, 2014; Tian and Dong, 2020), which tends to be most serious during boreal winter when the southern hemisphere receives its maximum amount of insolation. The double-ITCZ bias

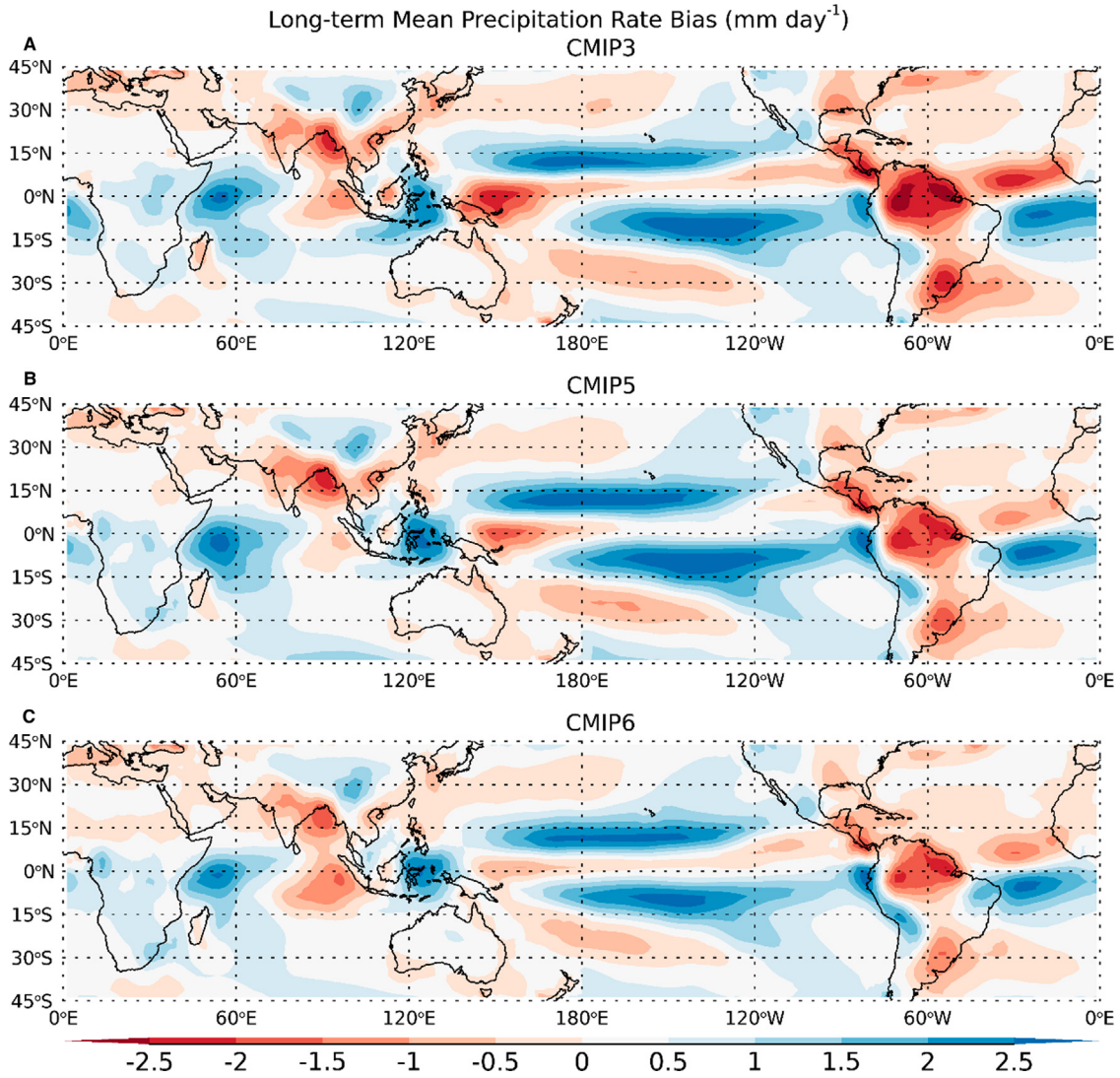

Fig. 12 Long-term annual mean precipitation bias (model−observation, mm day^{-1}) from the multi-model ensemble means of three recent generations of the World Climate Research Programme (WCRP) Coupled Model Inter-comparison Project (CMIP), (A) CMIP3, (B) CMIP5, and (C) CMIP6. For observations, the average of the Global Precipitation Climatology Project (GPCP) and Tropical Rainfall Measurement Mission (TRMM) surface precipitation data is used. Adapted from Tian and Dong (2020).

has been one of the most prominent tropical precipitation biases in coupled climate models since the beginning of their development. It has been persistent across several generations of models participated in the Coupled Model Intercomparison Project (CMIP), despite significant community efforts during the past decades towards improved simulations of the ITCZ through improved model resolutions, convection and cloud schemes, and land and ocean processes, etc. As shown in **Fig. 12** from Tian and Dong (2020), very similar patterns of precipitation biases over the ITCZ region are found in all three recent generations of CMIP models, i.e., CMIP3, CMIP5, and CMIP6. Along with the double-ITCZ biases in model simulations, persistent positive precipitation biases across the three generations of CMIP models are also found over the equatorial western Indian Ocean and the Maritime Continent, while negative precipitation biases over the equatorial north Atlantic (equator−5°N), the Central America, the Amazonia, the south Asia including the Bay of Bengal, and the equatorial western Pacific. This double-ITCZ bias is also evident in atmospheric models forced with the observed SST and sea ice, although it is much less severe than that in their corresponding coupled models.

The double-ITCZ bias not only affects models' simulation of the current climate, e.g., the large-scale Hadley circulations, and phenomena such as the MJO and ENSO as previously discussed, but also the models' climate sensitivity in response to the CO_2 induced radiative forcing (Tian, 2015; Webb and Lock, 2020). A climate model with more serious double-ITCZ bias tends to predict a weaker amplitude of global warming given the same CO_2 forcing, possibly due to a lack of a positive cloud-radiative feedback resulted from reduced low clouds over the southeastern Pacific and Atlantic (Webb and Lock, 2020).

Summary

Situated in the equatorial trough where surface trade winds converge to form a zone of heavy precipitation, the ITCZ plays a crucial role in the global energy and water cycles. The variability of the ITCZ on various time scales not only exerts impacts on climate and weather extremes worldwide but also influences the progress of global climate change. However, it remains a great challenge for the state-of-the-art climate models in realistically simulating the ITCZ and variability, noted as the so-called "double-ITCZ" biases. Further investigations are warranted towards improved understanding of the root causes of the double-ITCZ biases in climate models and modeling capability of representing the ITCZ and its global impacts.

References

Bessafi, M., Wheeler, M.C., 2006. Modulation of south Indian ocean tropical cyclones by the Madden-Julian oscillation and convectively coupled equatorial waves. Mon. Weather Rev. 134, 638–656.
Camargo, S.J., Wheeler, M.C., Sobel, A.H., 2009. Diagnosis of the MJO modulation of tropical cyclogenesis using an empirical index. J. Atmos. Sci. 66, 3061–3074.
Garfinkel, C.I., Feldstein, S.B., Waugh, D.W., Yoo, C., Lee, S., 2012. Observed connection between stratospheric sudden warmings and the Madden-Julian Oscillation. Geophys. Res. Lett. 39, L18807.
Hwang, Y.-T., Frierson, D.M.W., 2013. Link between the double-intertropical convergence zone problem and cloud biases over the southern ocean. Proc. Natl. Acad. Sci. U. S. A. 110, 4935–4940.
Jiang, X., Waliser, D.E., 2008. Northward propagation of the subseasonal variability over the eastern Pacific warm pool. Geophys. Res. Lett. 35.
Jiang, X., Li, T., Wang, B., 2004. Structures and mechanisms of the northward propagating boreal summer intraseasonal oscillation. J. Clim. 17, 1022–1039.
Jiang, X., Zhao, M., Waliser, D.E., 2012. Modulation of tropical cyclones over the eastern Pacific by the intraseasonal variability simulated in an AGCM. J. Clim. 25, 6524–6538.
Jiang, X., Adames, Á.F., Kim, D., Maloney, E.D., Lin, H., Kim, H., Zhang, C., DeMott, C.A., Klingaman, N.P., 2020. Fifty years of Research on the Madden-Julian oscillation: recent progress, challenges, and perspectives. J. Geophys. Res. Atmos. 125, e2019JD030911.
Kang, W., Tziperman, E., 2018. The MJO-SSW teleconnection: interaction between MJO-forced waves and the midlatitude jet. Geophys. Res. Lett. 45, 4400–4409.
Kosaka, Y., Xie, S.-P., 2013. Recent global-warming hiatus tied to equatorial Pacific surface cooling. Nature 501, 403–407.
Lawrence, D.M., Webster, P.J., 2002. The boreal summer intraseasonal oscillation: relationship between northward and eastward movement of convection. J. Atmos. Sci. 59, 1593–1606.
Lee, S., Gong, T., Johnson, N., Feldstein, S.B., Pollard, D., 2011. On the possible link between tropical convection and the northern hemisphere Arctic surface air temperature change between 1958 and 2001. J. Clim. 24, 4350–4367.
Li, G., Xie, S.-P., 2014. Tropical biases in CMIP5 multimodel ensemble: the excessive equatorial Pacific cold tongue and double ITCZ problems*. J. Clim. 27, 1765–1780.
Madden, R.A., Julian, P.R., 1971. Detection of a 40–50 Day oscillation in the zonal wind in the tropical Pacific. J. Atmos. Sci. 28, 702–708.
Maloney, E.D., Hartmann, D.L., 2000. Modulation of hurricane activity in the Gulf of Mexico by the Madden-Julian oscillation. Science 287, 2002–2004.
Nakazawa, T., 1988. Tropical super clusters within intraseasonal variations over the western Pacific. J. Meteorol. Soc. Japan 66, 823–839.
Sikka, D.R., Gadgil, S., 1980. On the maximum cloud zone and the ITCZ over Indian, longitudes during the southwest monsoon. Mon. Weather Rev. 108, 1840–1853.
Tian, B., 2015. Spread of model climate sensitivity linked to double-Intertropical Convergence Zone bias. Geophys. Res. Lett. 42, 4133–4141.
Tian, B., Dong, X., 2020. The double-ITCZ bias in CMIP3, CMIP5, and CMIP6 models based on annual mean precipitation. Geophys. Res. Lett. 47, e2020GL087232.
Wallace, J.M., Gutzler, D.S., 1981. Teleconnections in the geopotential height field during the northern hemisphere winter. Mon. Weather Rev. 109, 784–812.
Webb, M.J., Lock, A.P., 2020. Testing a physical hypothesis for the relationship between climate sensitivity and double-ITCZ bias in climate models. J. Adv. Model. Earth Syst. 12, e2019MS001999.
Wheeler, M.C., Hendon, H.H., 2004. An all-season real-time multivariate MJO index: development of an index for monitoring and prediction. Mon. Weather Rev. 132, 1917–1932.
Xie, S.-P., 2004. The shape of continents, air-sea interaction, and the rising branch of the Hadley circulation. In: Diaz, H.F., Bradley, R.S. (Eds.), The Hadley Circulation: Past, Present and Future. Kluwer Academic Publishers, Dordrecht, pp. 121–152.
Xie, S.-P., Kosaka, Y., 2017. What caused the global surface warming hiatus of 1998–2013? Curr. Clim. Change Rep. 3, 128–140.
Yasunari, T., 1979. Cloundiness fluctuations associated with the Northern Hemisphere summer monsoon. J. Meteorol. Soc. Japan 57, 227–242.
Yoo, C., Lee, S., Feldstein, S.B., 2012. Mechanisms of Arctic surface air temperature change in response to the Madden–Julian oscillation. J. Clim. 25, 5777–5790.

Further Reading

Emanuel, K.A., 1994. Atmospheric Convection. Oxford University Press, New York.
Gill, A.E., 1982. Atmosphere-Ocean Dynamics. Academic Press, Orlando, FL.
Kidder, S.Q., Vonder Haar, T.H., 1995. Satellite Meteorology: An Introduction. Academic Press, San Diego, CA.
Kraus, E.B., Businger, J.A., 1994. Atmosphere-Ocean Interaction. Oxford University Press, New York.
Lindzen, R.S., 1990. Dynamics in Atmospheric Physics. Cambridge University Press, Cambridge, UK.
Salby, M.L., 1996. Fundamentals of Atmospheric Physics. Academic Press, San Diego, CA.
Wallace, J.M., Hobbs, P.V., 2005. Atmospheric Science: An Introductory Survey, second ed. Academic Press, San Diego, CA.
Xie, S.-P., 2023. Coupled Atmosphere-Ocean Dynamics: From El Nino to Climate Change. Elsevier, Cambridge, MA.